NURETH14-468

VALIDATION OF STAR-CCM+ FOR BOUYANCY DRIVEN MIXING IN A PWR REACTOR PRESSURE VESSEL.

V. Petrov, A. Manera

Laboratory of Reactor Physics and System Behavior Paul Scherrer Institute, Switzerland victor.petrov@psi.ch; annalisa.manera@psi.ch

Abstract

Within the OECD/NEA PKL-II project, experiments have been carried out aimed at investigating the flow mixing in the downcomer and lower plenum of a pressurized water reactor (PWR) in the buoyancy driven mixing regimes. The experiments have been performed at the ROCOM test facility, a 1:5 scaled representation of a KONVOI type pressurized water reactor (PWR). The facility is equipped with advanced instrumentation (i.e. wiremesh sensors) allowing a detailed measurement of flow mixing in the downcomer annulus and at the core inlet. A computational fluid dynamic (CFD) model has been developed at the Paul Scherrer Institute within the STARS project [1], employing the STAR-CCM+code. The CFD model has been validated against the ROCOM experimental results. It has been shown that the developed model provided a good agreement with experiment. In order to evaluate the difference between momentum driven and density driven mixing regimes, calculations were performed assuming no density difference, and with 12% higher density in one of the loops respectively.

Introduction

With the current growing rate of availability of computational resources, and the improvements in turbulent modelling, the applications of CFD codes to reactor safety issues are increasing. CFD codes have become a valuable tool in order to gain physical insight in single-phase mixing mechanisms and accompanying effects [2]-[6]. In the field of nuclear engineering, single-phase mixing in the downcomer of the reactor pressure vessel (RPV) of a nuclear reactor plays an important role in nuclear power plant safety. Typical cases are boron dilution scenarios, characterized by a lower boron concentration in the affected loop, or main steam line breaks (MSLB), where the affected loop is characterized by a lower fluid temperature. Depending on the particular transient scenario, the dominant factors that influence the mixing in the downcomer and in the lower plenum of the RPV can have different nature. In transient scenarios where no or small temperature differences (i.e. no or small density differences) are experienced in the flow-rate entering the RPV from different loops, the mixing in the downcomer and lower plenum will be mainly driven by momentum. However, in case of transients where large temperature differences occur between the loops (i.e. in some MSLBs), the mixing can become buoyancy driven. Various experimental studies have been performed in order to evaluate mixing three-dimensional (3D) phenomena for different reactor types. At this aim different experimental facilities have been employed: ROCOM (Research Center Rossendorf-Dresden, Germany), VATT-02 (Vattenfall Utveckling AB, Alvkarleby, Sweden), BOMIX (Korea Atomic Energy Research Institute, Daejeon, Republic of Korea), VVER scale model (OKB "GIDROPRESS" Podolsk, Russia).

1. Experiment description

The ROCOM test facility models the primary circuit of a German KONVOI-type reactor in a linear scale of 1:5. The reactor pressure vessel was manufactured from acrylic glass and it forms the main part of the test facility. The geometrical similarity between the model and the original reactor is fully kept from the region upstream of the cold legs bends, which are closest to the reactor inlet, to the core entrance. The geometry of the inlet nozzles with their diffuser segments and the curvature radius of the inner wall at the junction with the pressure vessel were modeled in detail. Similarity is also taken into account for the core support plate, with the orifices for the coolant. The original KONVOI reactor has a perforated drum (flowskirt below the core barrel), which is also placed in the lower plenum of the vessel in the ROCOM test facility [7]. The experimental facility layout is indicated in Fig. 1.

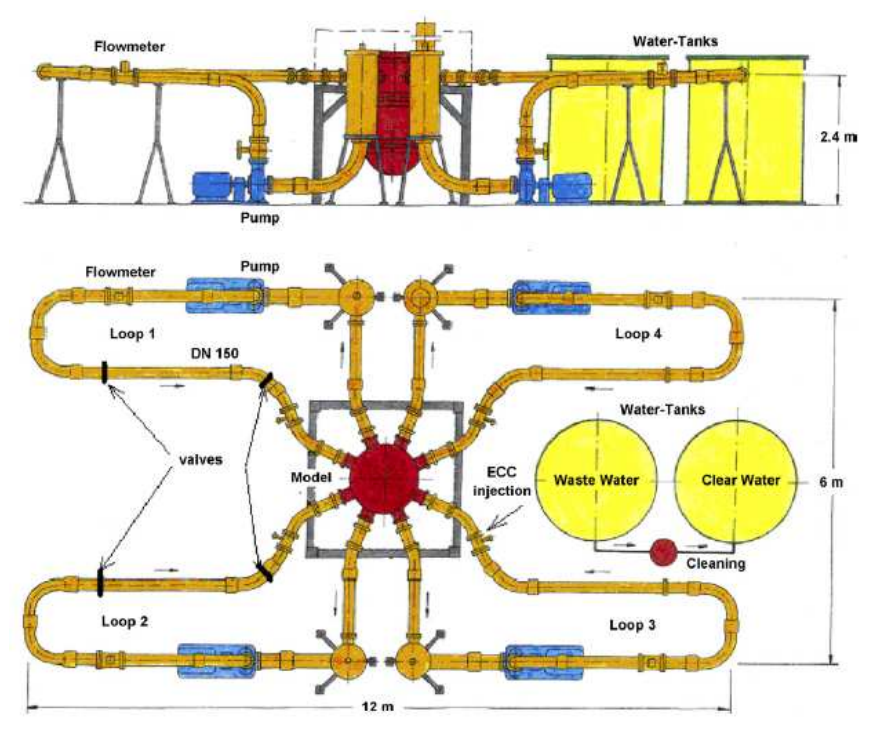


Fig. 1 Experimental facility layout.

The facility is operated with de-mineralized water at room temperature. Salt water or brine is used to alter the local electrical conductivity of the fluid in order to label a specific volume of water and thus simulate an under-borated slug of coolant. The distribution of this tracer in the test facility is measured by special wire-mesh electrical conductivity sensors developed at the Forschungszentrum Dresden-Rossendorf (FZD), which allows a high-resolution measurement both in space and time of the transient tracer concentration [8]. One sensor is integrated into the lower core support plate providing one measurement position at the entry into each fuel assembly. The downcomer is equipped with a measuring grid of 64 azimuthal and 29 axial positions [9]. In total more than 4000 measurement points are present in the facility.

In order to scale the buoyancy effects as in a real PWR RPV, the dimensionless similarity Froude criteria was adopted, in order to select the appropriate coolant flow rate. The Froude number is expressed as:

$$Fr = \sqrt{\frac{\rho \, w^2}{\Delta \rho g L}} \tag{1}$$

where g is the gravitational acceleration, ρ the water density, and $\Delta \rho$ is the density difference between pure and salted water; w and L are the coolant velocity and a characteristic length, respectively. On the basis of the expression given in (1), and taking into account the linear scaling of 1:5, the velocity in the ROCOM facility was reduced by a factor of $\sqrt{5}$ [7]. The boundary conditions of the experiments discussed in the present work correspond to the transients analyzed within the OECD/NEA PKL-II project for MSLB scenarios, and are summarized in Table 1.

Experiment boundary conditions.

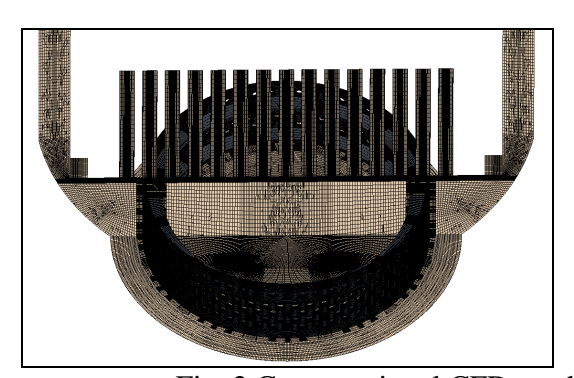
 Loop
 1
 2
 3
 4

 Normalized volume flow rate [-]
 3.876
 1.00
 1.00
 1.00

 Relative density [-]
 1.12
 1.00
 1.00
 1.00

2. Mesh

Two different types of meshes were developed, in order to create a full CFD model of the ROCOM facility. The first mesh type is hexahedral, while the second employs polyhedral elements (see Fig. 2). To simplify the development of a hexahedral mesh, the entire volume of the ROCOM facility included in the CFD model was divided into parts which could be meshed separately. Those parts were then duplicated by exploiting the symmetry or periodicity characteristics of the different parts. This applies for example to the perforated drum (shown in Fig. 3) present in the lower plenum, with more than 300 identical cylindrical holes, and to the reactor core channels, with 193 identical vertical pipes (see Fig. 4).



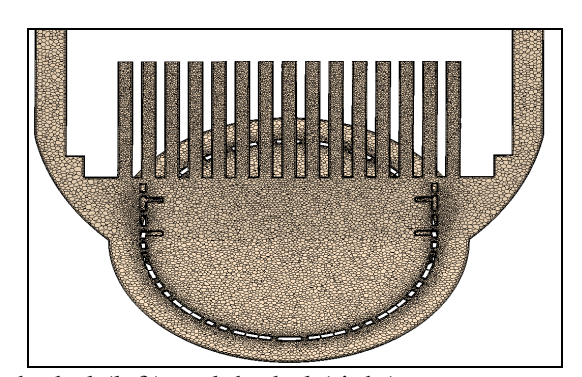


Table 1

Fig. 2 Computational CFD mesh: hexahedral (left), polyhedral (right).



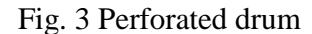




Fig. 4 Reactor core mock-up

Both hexahedral and polyhedral meshes exhibit lower numerical diffusion than a mesh with tetrahedral elements [10]. In a previous work [11], it has in addition been shown that for complex flow field such as the one which develops within the RPV, where the flow field does not present a dominant direction. polyhedral meshes yield better results than hexahedral meshes. The fact that polyhedral and hexahedral meshes are affected by lower numerical diffusion is of advantage for the correct prediction of the temperature field in the lower plenum, since it prevents the smoothing of the temperature gradients. However, for the test 1.1 analyzed in the present study (test 1.1), the temperature at the core inlet is almost uniform, and therefore numerical diffusion will not play a significant role. On the other hand, the reduction of numerical diffusion is important for other cases when the amount of injected cold (heavier) water is lower and the temperature stratification in the lower plenum is more evident.

Following the Best Practice Guidelines for the use of CFD in Nuclear Reactor Safety Applications [12], mesh sensitivity studies should be performed by applying one refining factor for the entire mesh in all directions. This guideline is still of not easy applicability when the overall size of the CFD model is large, due to the lack of appropriate computational resources. Therefore the influence of the cells size on the solution was examined separately for different parts of the CFD model.

Some parts of the experimental facility do not play any role for the CFD simulation, and can be neglected (e.g. all the piping behind the vertical channels which are replaced reactor core). Nevertheless, all geometric simplification should be carefully made: for example the vertical pipes which are replacing the reactor core do not need to be modeled in their full length, nevertheless a minimum length should be preserved in order to avoid the impact on the temperature values at core inlet of the boundary condition imposed at the core channels outlet.

The final polyhedral and hexahedral meshes contain approximately 6 millions and 10 millions of cells respectively (i.e. the polyhedral mesh is considerably smaller than the hexahedral one). As a matter of fact, in some regions fewer amounts of polyhedral cells can provide a more uniform cell distribution than hexahedral cells (see Fig. 5).

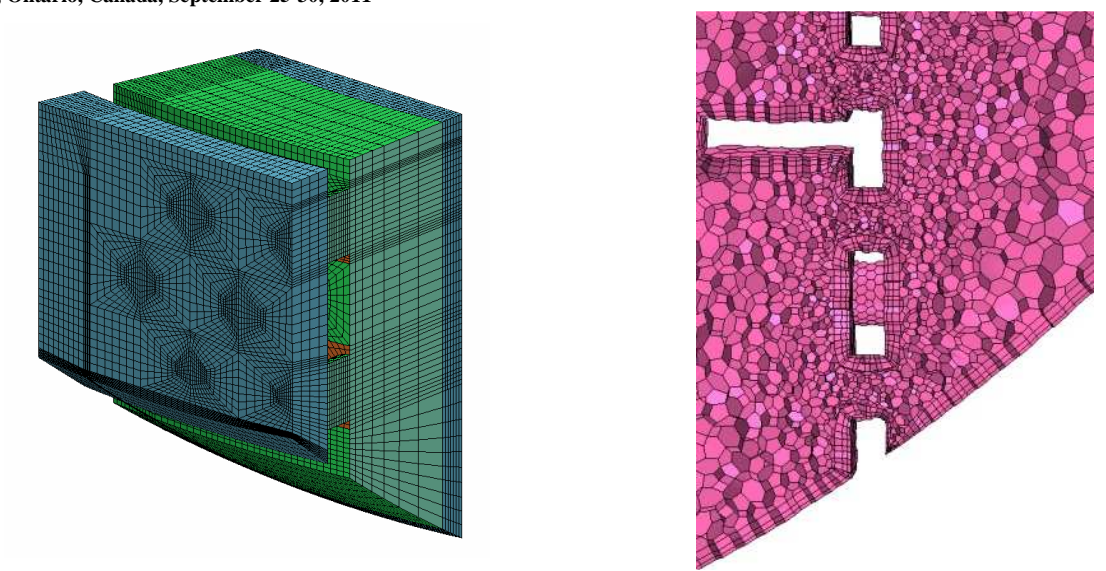


Fig. 5 Mesh in perforated drum section: hexahedral (left), polyhedral (right).

3. CFD model

All the calculations discussed in the present work have been performed by employing the realizable k- ϵ two-layer turbulence model [13]. The buoyancy effect was modeled adopting the Boussinesq approximation. In this case, buoyancy source term in the momentum balance equation is written as follow:

$$f_{g} = \rho g \beta (T_{ref} - T)$$
 (2)

where: T_{ref} - T is the temperature difference, and β is the coefficient of bulk expansion. The value of β was selected such to take into account a 12% higher density in the first loop with respect to the remaining three loops. The Boussinesq approximation is valid when:

$$\beta T_{ref} - T < 1$$

Inlet boundary conditions with imposed mass flow rate were used for all the four loops. For the first 30 seconds of transient, no flow was circulating in loop 1. After 30s of transient, the injection of cold water in loop 1 was started. A scheme of the boundary conditions applied to the CFD model is reported in Fig. 6.

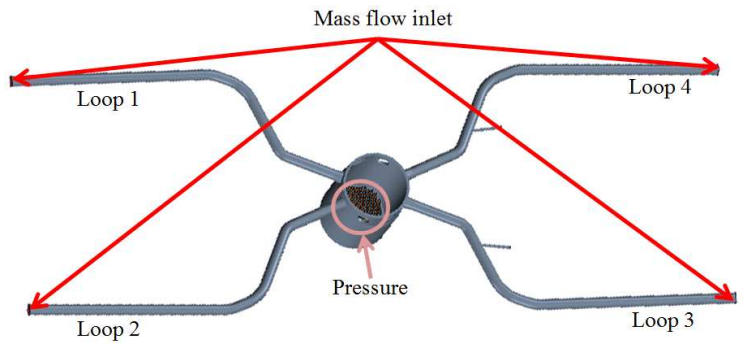


Fig. 6 CFD model.

4. Calculation results

In order to investigate buoyancy effects in the mixing patterns in the downcomer and lower plenum, two different cases were calculated:

- No density difference between loops flow (mixing is momentum driven);
- 12 % density differences (mixing is mostly buoyancy driven).

First order discretization scheme in time and second order upwind discretization scheme in space were adopted for the calculation with a constant time step of 0.01 s. The simulations convergence of the full CFD model was first analysed by performing steady-state calculations. The boundary conditions for the loops flow-rates were imposed according to the experimental values. The results of the converged studies are presented in Fig. 7 (left and center). It can be noticed that the polyhedral mesh results in a higher level of residuals compared to the hexahedral one. However, the convergence of the polyhedral mesh solution improved considerably when the CFD code is executed in transient mode (see Fig. 7, right), with 20 internal iterations per each time step.

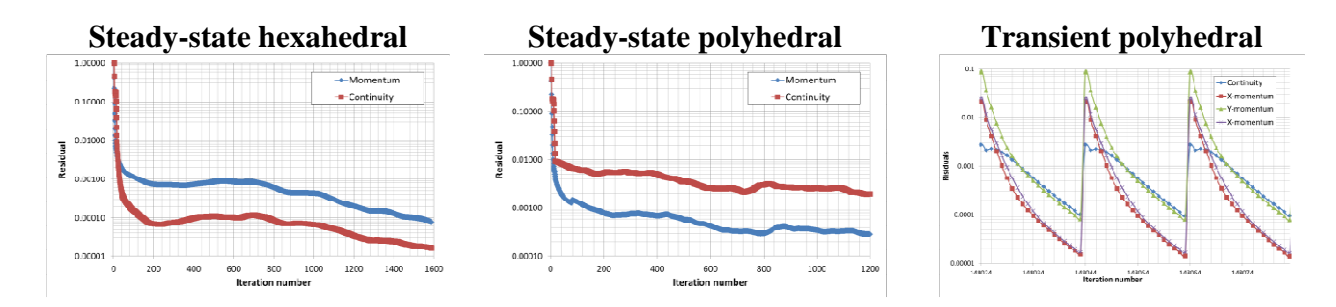


Fig. 7 Simulations convergence.



Fig. 8 Flow streamlines with no density difference (left) and 12% density difference (right). The colour bar represents the velocity magnitude.

The stream lines of the flow patterns for the cases with no density difference and 12% density difference are shown in Fig. 8 respectively. It is evident that in case of non-buoyant flow the fluid arriving from the first loop flows around the downcomer, before reaching the lower plenum at a certain angular distance from the loop 1 inlet location. This is caused by the higher mass flow-rate in loop 1 with respects to the other loops. The angular distance will actually depend on the difference in mass flow rate between first loop and its neighbors (loop 2 and 4). When the effect of density difference is

dominant, as in the second case, the axial component of the velocity is prevailing, enforcing the flow to go downwards into the downcomer annulus, as can be observed in Fig. 8 (right). The normalized temperature fields in the downcomer are presented in Fig. 9. In the figure, the measured and calculated temperature values along the elevation and the circumference of the unwrapped downcomer are shown. The location of the cold legs (CL1 to CL4) is indicated as well. The phenomenological difference of temperature distribution in case of no density difference and 12% density difference can be clearly observed. The simulation results for 12% density difference is qualitatively in very good agreement with the experimental trends, though differences in local effects can be seen, especially in zones with small perturbations. In addition, the temperature of the plume kernel is over predicted. The temperature distribution at the core inlet 34s after the injection of the cold flow is reported in Fig. 10. Both the experimental values, as the corresponding simulation (12%) show an almost uniform temperature distribution. This is not the case when a non-buoyant flow is considered (see Fig. 10, left): the mixing between the cold plume with the flows from the other three loops taking place in the downcomer and lower plenum is not high enough to prevent colder water from reaching the core inlet.

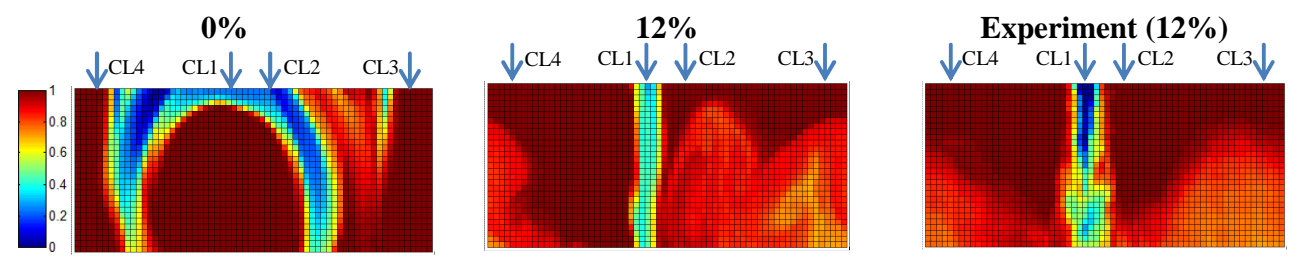


Fig. 9 Temperature in outer side of downcomer (20 second after cold water injection started).

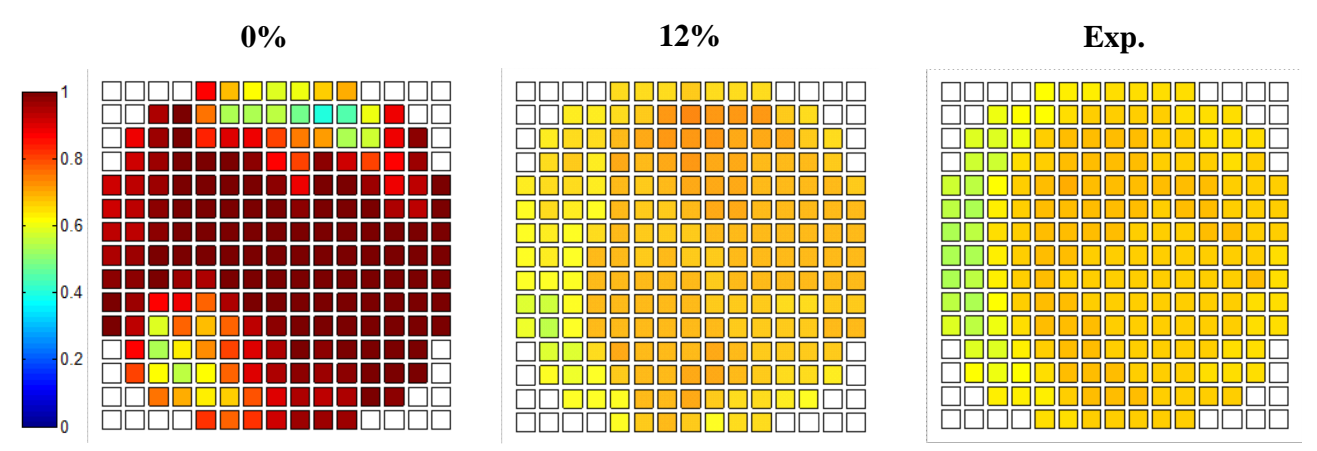


Fig. 10 Temperature at the core inlet (34 seconds after injection started)

In order to provide a quantitative comparison as well, three sets of measurement locations were selected at the elevation of the core inlet for comparison between simulation results and experimental data. The first set of sensors (set 1) is selected in the outer region of the core inlet, situated outside the zone of the perforated drum, the sensors belonging to set 2 are situated in the core region just above the perforated drum, while the sensors within set 3 are situated in the central region of the core. The selected sensors are indicated in Fig. 11. The experimental time traces of the temperature measured for sets 1, 2 and 3 are reported in Fig. 12 to Fig. 14 respectively, together with the simulation results. Good agreement with the experimental data is obtained. The CFD results present higher temperature fluctuations in the proximity of loop 1 (the affected loop) and 2 (see Fig. 12) with respect to loop 3 and 4. Also, the intensity of these fluctuations decreases when approaching the core center. It can be concluded that the

strong temperature gradient in the region below loop 1 and 2 induces local temperature fluctuations. The amplitude of those fluctuations decays approaching the center of the lower plenum. The cross-section averaged core inlet temperature is presented in Fig. 15. It can be seen that the CFD model (with 12% density difference) is able to correctly capture the decrease of core inlet average temperature as function of time. In Fig. 15, the temperature evolution in case the mixing would be momentum driven (case with 0% density difference) rather than buoyancy driven is also reported. In Fig. 16 the measurements and corresponding simulation results for monitoring points close to the outer wall of downcomer are presented. These monitoring points are located in the middle of the downcomer elevation, as illustrated in Fig. 16 (left). Not all temperature oscillations are captured by the CFD model Fig. 16 (right), especially for the monitoring points situated below loops 3 and 4, indicating that some local vortexes are not well captured by the turbulence model. Also from the data of monitoring point situated below loop 1 could be concluded, that applying lower value of the time step may improve the resolution of the calculation. Further investigations on buoyancy induced turbulence production are necessary.

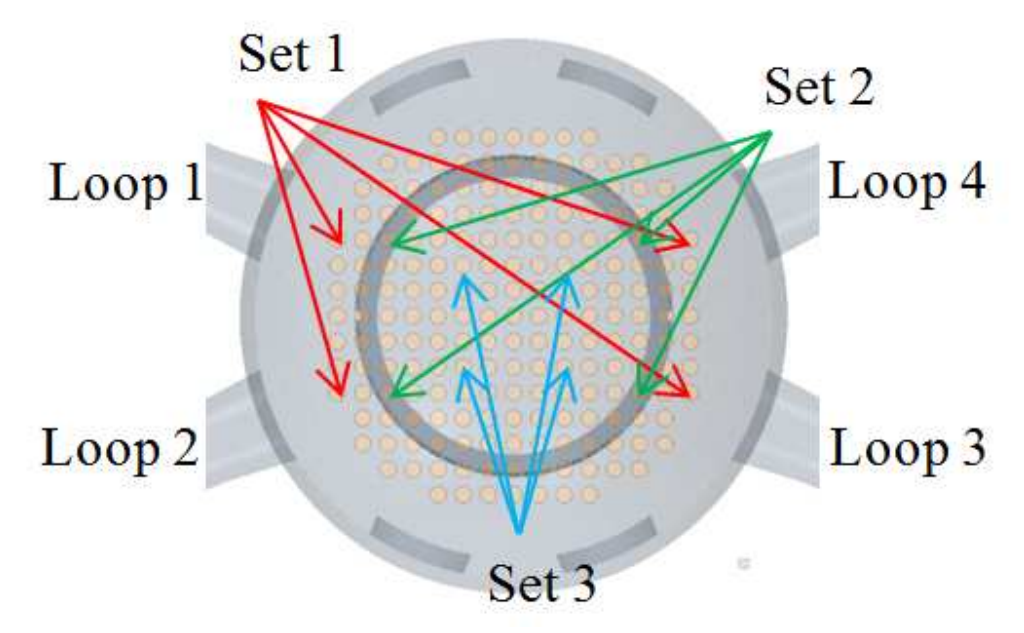


Fig. 11 Sensors positions.

The 14th International Topical Meeting on Nuclear Reactor Thermalhydraulics, NURETH-14 Toronto, Ontario, Canada, September 25-30, 2011

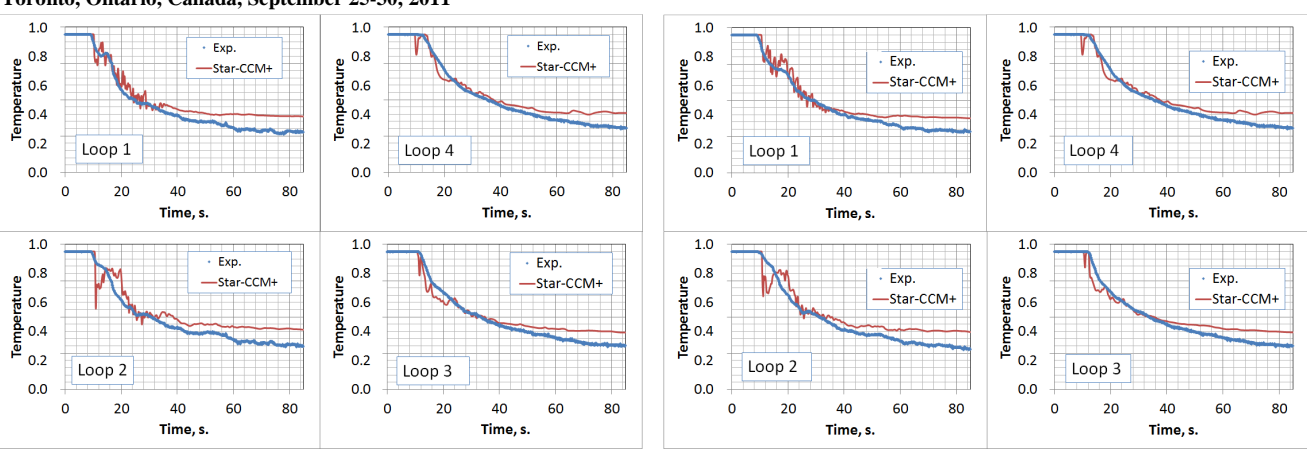


Fig. 12 Core inlet temperature for sensors in Set1.

Fig. 13 Core inlet temperature for sensors in Set2.

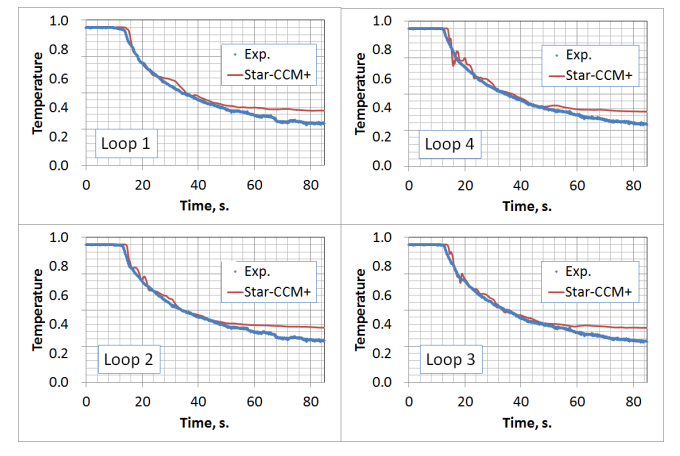


Fig. 14 Core inlet temperature for sensors in Set3.

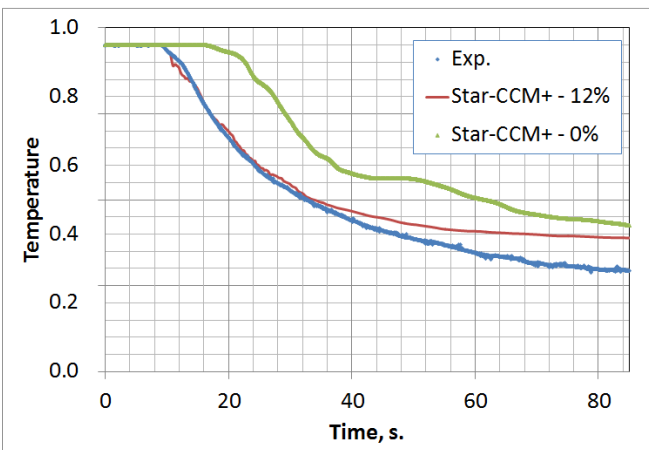
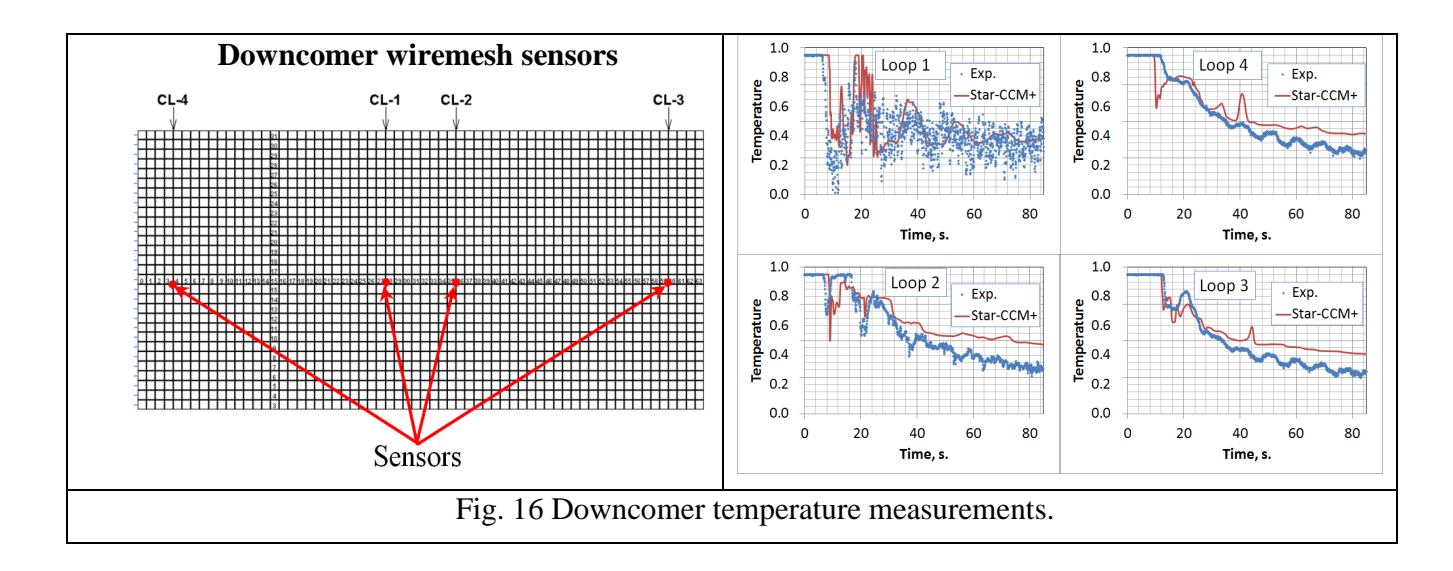


Fig. 15 Average Core inlet temperature evolution.



5. Conclusion

In the present work a full CFD model of the ROCOM experimental facility has been created, adopting two different mesh types, a hexahedral and a polyhedral mesh respectively. Computation results obtained with the polyhedral mesh have shown that the CFD model is correctly able to capture qualitatively as well as quantitatively the time evolution of the temperature distribution at the core inlet, when considerable density differences exist between the loops flow-rate. An additional simulation carried out neglecting the buoyancy effects, shows significant differences in the mixing mechanism when the mixing is momentum driven, rather than buoyancy driven. The average temperature at the core inlet has a similar trend, but with a delay in time, for momentum driven mixing. The local temperature distribution, on the other hand, is strongly affected by the dominant mixing mechanism. The presence of temperature oscillations, especially the one detected at the monitoring points situated in the outer part of the core inlet plane, are an indication that vortexes generated in the lower plenum are not well predicted by the CFD model. In order to improve the computational results, a more advanced turbulence model able to take into account anisotropic effects should be adopted. This will be part of future investigations.

6. Acknowledgments

This work was performed within the framework of the STARS project (http://stars.web.psi.ch) and was partly funded by the Swiss Federal Nuclear Safety Inspectorate ENSI (Eidgenössisches Nuklearsicherheitsinspektorat). This paper contains findings that were produced within the OECD-PKL-2 Project. The authors are grateful to the participants and the Management Board of the OECD-PKL-2 Project for their consent to this publication.

7. References

- [1] http://stars.web.psi.ch/
- [2] H. Tinoco, "Three-dimensional modeling of a steam-line break in a boiling water reactor", Nucl. Techn., 140, 152-164, 2002.
- [3] T.-S. Kwon, C.-R. Choi, C.-H. Song, "Three-dimensional analysis of flow characteristics on the reactor vessel downcomer during the late reflood phase of a postulated LBLOCA", Nucl. Eng. Des., 226, 255-265, 2003.
- [4] U. Bieder, G. Fauchet, S. Betin, N. Kolev, D. Popov, "Simulation of mixing effects in a VVER-1000 reactor", Nucl. Eng. Des., 237, 1718-1728, 2007.
- [5] E. Popov, B. Ivanov, K.N. Ivanov, S. Miladenova, "Simulation of the flow rotation and mixing in the downcomer of a VVER-1000 reactor", Nucl. Techn., 158, 358-365, 2007.
- [6] J.H. Jeong, B.-S. Han, "Coolant flow field in a real geometry of PWR downcomer and lower plenum", Annals of Nucl. Energy, 35, 610-619, 2008.
- [7] S. Kliem, H.-M. Prasser, T. Suhnel, F.-P. Weiss, A. Hansen, 2008. Experimental determination of the boron concentration distribution in the primary circuit of a PWR after a postulated cold leg small break loss-of-coolant-accident with cold leg safety injection. Nucl. Eng. And Design 238, 1788-1801. 2008
- [8] Prasser, H.-M., Böttger, A., Zschau, J., 1998. A new electrode-mesh tomograph for gas-liquid flows. Flow Meas. Instrum. 9, 111–119.
- [9] S. Kliem, T. Höhne, U. Rohde, F.-P. Weis, "Experiments on slug mixing under natural circulation conditions at the ROCOM test facility using high-resolution measurement techniques and numerical modeling" Nucl. Eng. And Design 240, 2271-2280. 2010.
- [10] C. Moulinec, S. Benhamadouche, D. Laurence M. Peric. LES in a U-bend pipe meshed by polyhedral cells. ERCOFTAC ETMM-6 conference, Sardinia, Mai 2005, Elsevier.
- [11] V. Petrov, A. Manera, "Effect of pump-induced cold-leg swirls on the flow field in the RPV of the EPRTM: CFD investigations and comparison with experimental results", accepted for publication in Nucl. Eng. And Design, 2011.
- [12] NEA, "Best Practice Guidelines for the use of CFD in Nuclear Reactor Safety Applications", NEA/CSNI/R(2007)5, April 2007.
- [13] Rodi, W. "Experience with Two-Layer Models Combining the k-e Model with a One-Equation Model Near the Wall", 29th Aerospace Sciences Meeting, January 7-10, Reno, NV, AIAA 91-0216. 1991.